Eur. Phys. J. B **9**, 71–82 (1999)

THE EUROPEAN PHYSICAL JOURNAL B

EDP Sciences

Dynamic and static light scattering study of the formation of cross-linked PMMA gels

V. Lesturgeon, T. Nicolai[a], and D. Durand

Chimie et Physique des Matériaux Polymères[b], Université du Maine, 72085 Le Mans Cedex 9, France

Received 11 May 1998 and Received in final form 22 October 1998

Abstract. Free radical co-polymerization of methyl methacrylate (MMA) and ethyl glycol dimethyl metacrylate (EGDMA) was investigated in solution at different molar ratios R = [EGDMA]/[MMA] between 0 and 0.05. Initially mainly linear PMMA was formed with weight average molar mass 7.5×10^4 g/mol independent of R. At larger reaction extents branched polymers were formed and the systems gelled. The scattering intensity rose initially with the reaction extent, but reached a plateau value at larger reaction extents. The plateau value increased strongly with R. Dynamic light scattering showed the appearance of a slow relaxation not observed in linear PMMA solutions. The data can be interpreted by assuming that the excess scattering originates from the branching points and relaxes through self diffusion of the branched particles. The results agree with predictions of the percolation model for gelation and Rouse dynamics. Viscosity measurements corroborate this interpretation. Measurements on a progressively diluted sample quenched close to the gel point again showed quantitative agreement with the percolation model for gelation.

PACS. 36.20.-r Macromolecules and polymer molecules – 61.10.-i X-ray diffraction and scattering – 82.70.Gg Gels and sols

1 Introduction

Scattering techniques have proven to be a useful tool to investigate the structural properties of polymers in solution. The application to gel forming systems is, however, in most cases not straightforward even if we limit our discussion to semi-dilute gels consisting of large weakly cross-linked flexible chains. A recent thorough review of static scattering properties was given by Bastide and Candau [1]. For large weakly cross-linked flexible linear chains an analogy exists with semi-dilute polymer solutions. If we can neglect the scattering by the cross-links, the only difference of such gels with semi-dilute solutions is the presence of a non-relaxing elastic modulus in addition to the osmotic modulus. As a consequence the time averaged amplitude of the polymer concentration fluctuations, which cause the scattering, is reduced. One therefore expects a reduction of the time-averaged scattering intensity with increasing cross-link density. In practice, however, almost always a larger scattering intensity is observed. Two possible origins of the excess scattering have been discussed in the literature. One is that cross-linking reduces the osmotic modulus and thus increases the amplitude of the concentration fluctuations. This effect has been shown to exist but is not enough to explain the sometimes very strong increase of the scattering intensity. The other possible origin is scattering by branching points, *i.e.* the cross-linking agent and the locally increased concentration of polymer segments. The strength of the additional scattering due to branching points can vary strongly from system to system depending on the scattering contrast of the branching points and their partition in the system; the more inhomogeneous their partition is the stronger is the scattering.

The dependence of the scattering intensity on the scattering wave-vector (q) reflects the presence of two length scales: the length scale over which polymer segment concentration fluctuations are correlated (ξ_p) and the one over which branching point concentration fluctuations are correlated (ξ_b). For weakly cross-linked flexible chains in good solvent the elastic modulus is small compared to the osmotic modulus so that ξ_p is close to the corresponding value for an uncross-linked solution with the same polymer concentration. ξ_b, is larger than ξ_p and is system dependent.

Dynamic light scattering (DLS) has been less often used to study gels [2]. A fast diffusive mode is often observed with a diffusion coefficient close to that of the corresponding semi-dilute solution. In addition, a slow mode is almost always observed which is possibly due to the relaxation of concentration fluctuations of the branching points. The relative amplitude of this mode is strongly system dependent varying from negligible to dominating. Its relaxation is characterized by a broad distribution of

[a] e-mail: nicolai@univ-lemans.fr
[b] UMR CNRS

relaxation times which can be very slow. If the relaxation is slower than the duration of the experiment, the time averaged scattering intensity is no longer the same as the ensemble averaged intensity and the system is non-ergodic. Non-ergodic scattering is the rule rather than the exception for gels. In strongly cross-linked gels the relative motion of branching points is inhibited and almost all the scattering from branching points is non-ergodic. Even in weakly cross-linked gels part of the branching point concentration fluctuations relax very slowly and it is in practice most often not possible to study these dynamics by DLS. However, branching points are formed already before the sol-gel transition and it is possible to study the dynamics of the branching points close to the gel point.

It has been observed that the scattering intensity increases strongly if a gel is swollen in a good solvent [1]. Dilution of semi-dilute solutions of linear polymers also leads to an increase of the scattering intensity, but the concentration dependence is moderate compared to what is usually observed in gels. If it is true that the cross-linked system is characterized by two length scales then both are expected to increase upon dilution, but not necessarily with the same concentration dependence. If ξ_p becomes much larger than the average distance between cross-links one might expect ξ_p and ξ_b to become equal so that the system is characterized by a single correlation length. DLS gives us the possibility to measure the effect of dilution on both contributions. Dilution of a gel is limited by the equilibrium swelling ratio. However, just before the gel point we can dilute the system indefinitely.

The object of the present paper is to investigate the properties of a typical polymeric gel, PMMA cross-linked with EGDMA, during the gel formation using static and dynamic light scattering. By varying the molar ratio R = [EGDMA]/[MMA] we studied the effect of the branching point density. In addition, we investigated the effect of dilution for a single sample very close to, but before the gel point. In a separate article [3] we give a characterization of the structure and the size distribution of the branched polymers that are formed at different stages of the gel formation before the gel point. A study of the size distribution using size exclusion chromatography (SEC) of a system with $R = 0.01$ was reported in reference [4]. We will use some of the results from that characterization to interpret the findings reported here.

2 Experimental

Solutions were prepared by dissolving the required amounts of MMA and EGDMA (Merck) in freshly distilled toluene or THF. 1.1×10^{-3} g/ml AIBN was added to initialize the reaction. The solutions were filtered through 0.2 μm pore size Anotop filters.

Static and dynamic light scattering measurements were made using an ALV-5000 multi-bit multi-tau correlator in combination with a Malvern goniometer and a Spectra Physics argon ion laser operating with vertically polarized light with wavelengths $\lambda = 488$ nm or 514.5 nm.

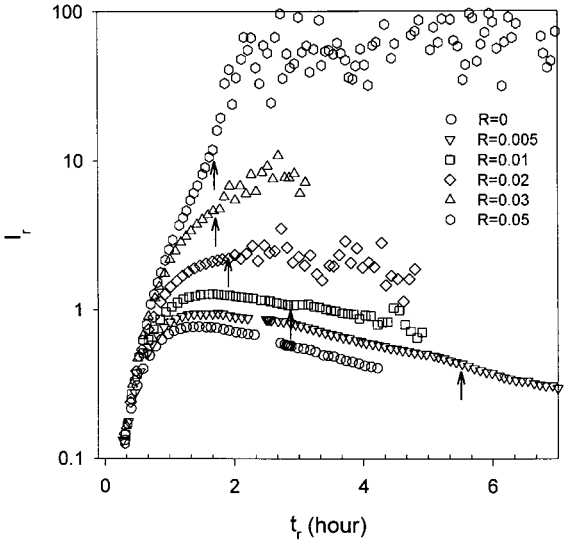

Fig. 1. Dependence of the excess scattering intensity ($I_r = (I - I_{sol})/I_{tol}$) on the reaction time of solutions containing MMA and various amounts of cross linker EGDMA (R = [EGDMA]/[MMA]) as indicated in the figure. The data are obtained from measurements at $q = 1.5 \times 10^{-2}$ nm^{-1}. The arrows indicate the gel points.

The temperature was controlled within $\pm 0.1\,^{\circ}$C using a thermostat bath.

3 Results

3.1 Static light scattering

We studied the free radical polymerization of MMA and EGDMA in toluene at $T = 68 \pm 0.1\,^{\circ}$C. Under the present experimental conditions free radical polymerization of MMA leads to the formation of linear PMMA chains with weight average molar mass 7.5×10^4 g/mol and polydispersity index $M_w/M_n = 2$. We varied the molar ratio R = [EGDMA]/[MMA] between 0 and 0.05 keeping the total concentration constant at 0.26 g/g. Figure 1 shows the excess scattering intensity relative to the scattering of toluene at 20 °C ($I_r = (I - I_{sol})/I_{tol}$) as a function of reaction time at different values of R. The solvent scattering (I_{sol}) was taken as the scattering of the system before the reaction started. In principle I_{sol} varies with reaction time as the composition of the solvent evolves from a mixture of MMA and toluene to pure toluene at the end of the reaction. However, the effect is negligible as the scattering of MMA is close to that of toluene. The reaction time (t_r) is defined as the total time elapsed at the reaction temperature minus the time needed to consume all the inhibitor present in the system. We measured the reaction extent (r) as a function of reaction time by Raman spectroscopy using the method described in [5]. These measurements show that r increases linearly with t_r independent of R in the range investigated: $r = 0.10 t_r$, with t_r in hours. This relation is valid at least up to the gel point and at least up to $t_r = 5$ hours for the uncross-linked system.

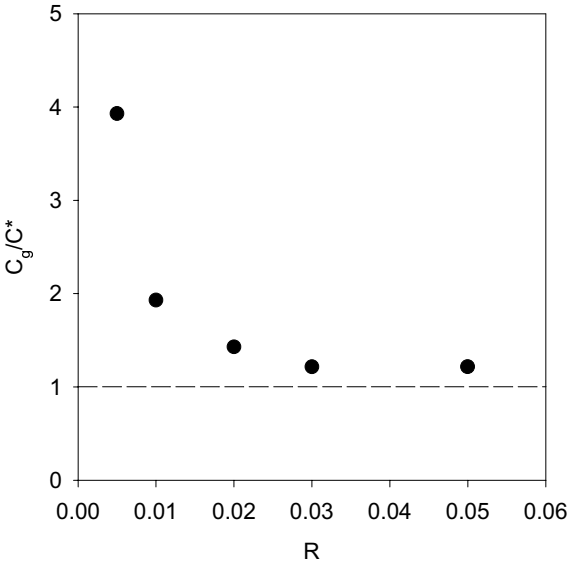

Fig. 2. PMMA concentration at the gel point (C_g) as a function of the molar ratio [EGDMA]/[MMA]. C_g is normalized by the overlap concentration $C^* = 0.035$ g/ml.

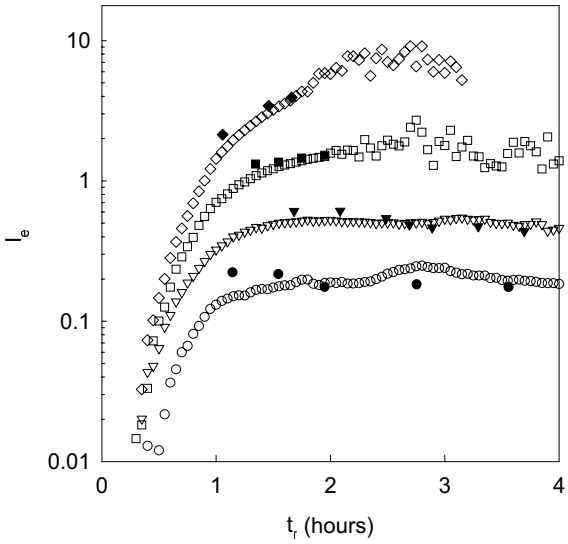

Fig. 3. Open symbols represent the excess scattering intensity of solutions containing MMA and various amounts of cross linker EGDMA (R = [EGDMA]/[MMA]) over solutions containing no cross linker ($I_e = (I(R) - I(R = 0))/I_{tol}$) as a function of reaction time. Closed symbols represent the contribution of mode 3 to $I_r = (I - I_{sol})/I_{tol}$.The data are obtained from measurements at $q = 1.5 \times 10^{-2}$ nm^{-1}. Symbols as in Figure 1.

The data shown in Figure 1 were measured at scattering wave vector $q = 1.5 \times 10^{-2}$ nm^{-1} ($q = (4\pi n_s/\lambda)\sin(\theta/2)$, n_s and θ being the solvent refractive index and the angle of observation, respectively). However, in all cases the q-dependence of I_r is small over the q-range accessible to light scattering techniques ($< 10\%$).

I_r increases rapidly at the beginning of the reaction, then reaches a maximum after which it decreases slowly or remains constant. At the very early stage of the reaction the increase of I_r is the same with and without cross-linker. SEC shows that initially mainly linear chains are formed with the same molar mass independent of R [3,4]. For $t_r > 30$ min the larger is R the stronger is the increase of I_r, which is obviously due to branching. For linear chains, *i.e.* $R = 0$, it is well-known that a maximum occurs in the concentration dependence of I_r at about the overlap concentration C^*. The overlap concentration of linear PMMA can be estimated as the inverse of the intrinsic viscosity: $C^* \approx [\eta]^{-1}$. From measurements in benzene reported in reference [6] we estimate that $[\eta] \approx 30$ ml/g and obtain $C^* \approx 0.033$ g/ml, which corresponds to $r \approx 0.14$. In the experiment we observe that I_r at $R = 0$ has a maximum at $t_r \approx 1.3$ hours which corresponds to $r \approx 0.13$.

The gel points are indicated by arrows in Figure 1. Here we define the gel point as the reaction time where the system no longer flows when tilted. The sol-gel transition is very abrupt so that different methods to determine the gel point will give approximately the same gel time. For the system with $R = 0.005$ the gel point was not determined, but at the end of the measurement at 430 min a gel was formed. Based on the increase of the terminal relaxation time (see below) we estimate the gel point for this sample at about 330 min. The PMMA concentration at the gel point (C_g) is plotted as a function R in Figure 2. We normalized C_g by C^* to show the degree of overlap of PMMA chains at the gel point. For $R = 0.005$ the gel is formed in a system with strongly overlapping PMMA chains and is therefore close to the case of vulcanization. C_g decreases with increasing cross-link ratio as expected for the case of vulcanization. The average number of cross-linker per PMMA chain varies from 1.8 at $R = 0.005$ to 18 at $R = 0.05$. However, C_g stabilizes at a value close to C^* for $R > 0.02$. This can be understood by realizing that branching is not enough to form a gel. Cross-links have to be created between branched particles. The probability of inter-particle instead of intra-particle cross-linking is small below C^* independent of R.

After the gel point the time averaged intensity fluctuates slowly in time. The amplitude of these fluctuations depends on the period over which each value of I_r is averaged (100 s for the data shown in Fig. 1). For a given averaging period the amplitude of the fluctuations increases with increasing R and t_r. However, the systems remain ergodic, *i.e.* the effect of turning the sample is not visible in Figure 1, although it leads to drastic immediate changes of the intensity. The system with $R = 0.05$ is an exception because variations in the sample position give somewhat larger variations of I_r than the fluctuations in time. For $R \geq 0.02$ the very slow fluctuations appear abruptly at the gel point. For the system with $R = 0.01$ the fluctuations develop gradually after the gel point while for the system with $R = 0.005$ no slow fluctuations were observed.

The excess scattering of the cross-linked systems over the uncross-linked system ($I_e = I_r(R) - I_r(R = 0)$) is plotted in Figure 3. I_e increases sharply at $t_r \approx 30$ min

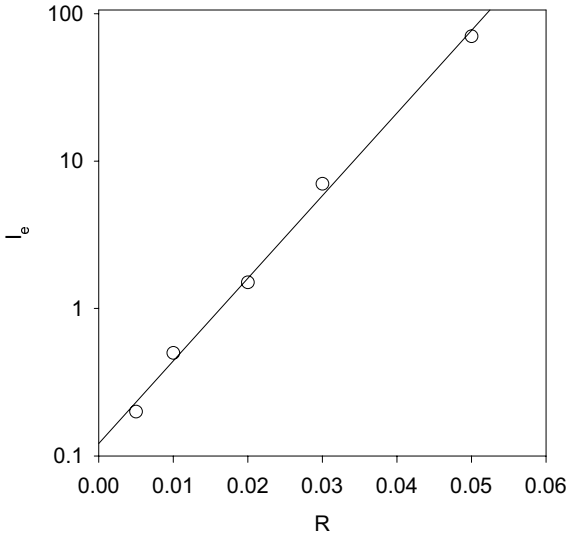

Fig. 4. Plateau values of the excess scattering intensity ($I_e = (I(R) - I(R=0))/I_{tol}$) shown in Figure 3 as a function of the molar ratio [EGDMA]/[MMA].

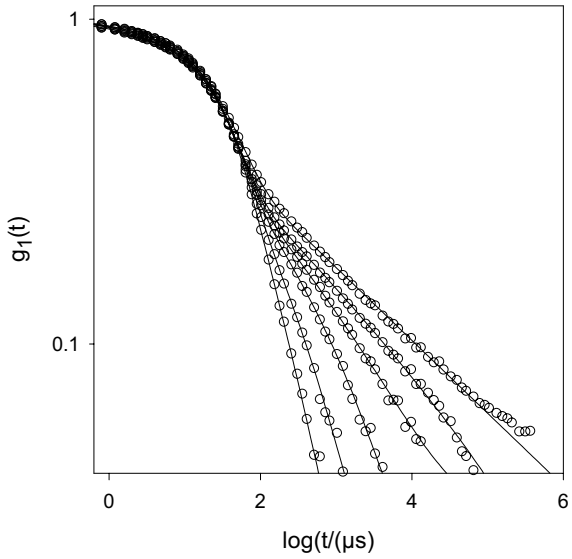

Fig. 5. Double logarithmic representation of the normalized electric field autocorrelation functions of a solution containing MMA and EGDMA with molar ratio $R = 0.01$ at different reaction times between 125 and 200 min. Solid lines are non-linear least squares fits to model *b*, see Appendix A.

but reaches a constant value at longer reaction times. The plateau value of I_e increases almost exponentially with R in the range investigated, see Figure 4.

3.2 Dynamic light scattering

We measured intensity autocorrelation functions for set periods of 10 min during the reaction. For scattering with Gaussian statistics the normalized intensity correlation function ($g_2(t)$) is related to the normalized electric field autocorrelation function ($g_1(t)$) [8]:

$$g_2(t) = 1 + g_1(t)^2. \quad (1)$$

Figure 5 shows $g_1(t)$ at different reaction times between 125 and 200 min for the system with $R = 1$.

During the early stages of the reaction the variation of I_r over a period of 10 min is not negligible which gives rise to a base line on $g_2(t)$. Close to, but before the gel point the variation of I_r is small over a period of 10 min (at least for $R < 0.03$) and the base line is negligible. Three relaxation processes can be distinguished which we will call modes 1, 2 and 3 in order of increasing relaxation time, see Figure 15 of the Appendix A. Mode 1 is already observed before the reaction and is due to the cooperative diffusion of MMA in toluene. The relative amplitude of this mode (A_1) decreases rapidly with increasing reaction time and is less than 0.1 for $t_r > 50$ min. Mode 2 is due to the cooperative diffusion of PMMA and is more than a factor 10 slower than mode 1. Mode 3 is only observed if EGDMA is added and it can be clearly distinguished from mode 2 at times close to and beyond the gel point. This mode covers a time range starting from the relaxation time of the mode 2 (τ_2) to a terminal relaxation time (τ_r) which increases with increasing reaction time. Close to the gel point mode 3 has an initial power law time dependence, *i.e.* a straight line in a log-log representation.

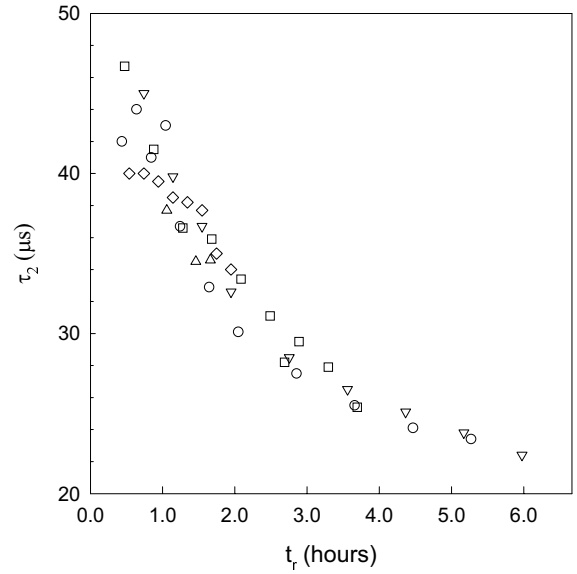

Fig. 6. Dependence of the average relaxation time of PMMA concentration fluctuations (mode 2) on the reaction time of solutions containing MMA and various amounts of cross linker EGDMA (R = [EGDMA]/[MMA]). The data are obtained from measurements at $q = 1.5 \times 10^{-2}$ nm^{-1}. Symbols as in Figure 1.

For reasons outlined below we believe that this mode is due to concentration fluctuations of branching points. As mentioned above, beyond the gel point very slow intensity fluctuations appear for $R > 0.005$. These slow fluctuations give rise to a base line of varying amplitude.

For a more quantitative analysis we used three methods which are detailed in the appendix. All three methods give the same values of the relaxation times of modes 1 and

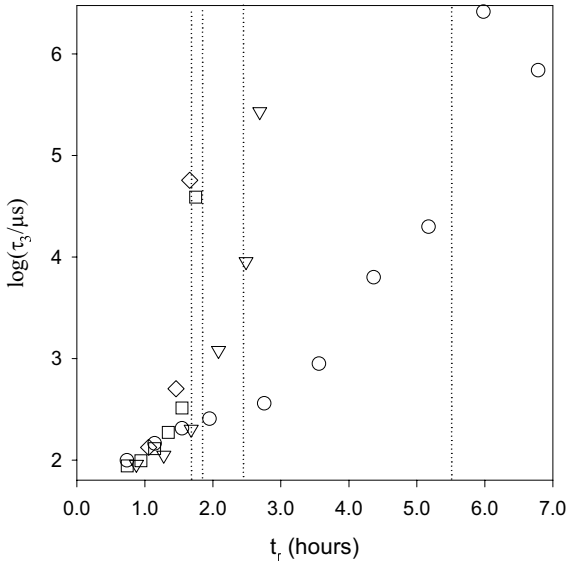

Fig. 7. Dependence of the average relaxation time of mode 3 on the reaction time of solutions containing MMA and various amounts of cross linker EGDMA (R = [EGDMA]/[MMA]). The data are obtained from measurements at $q = 1.5 \times 10^{-2}$ nm^{-1}. Symbols as in Figure 1. The dashed lines represent the gel time.

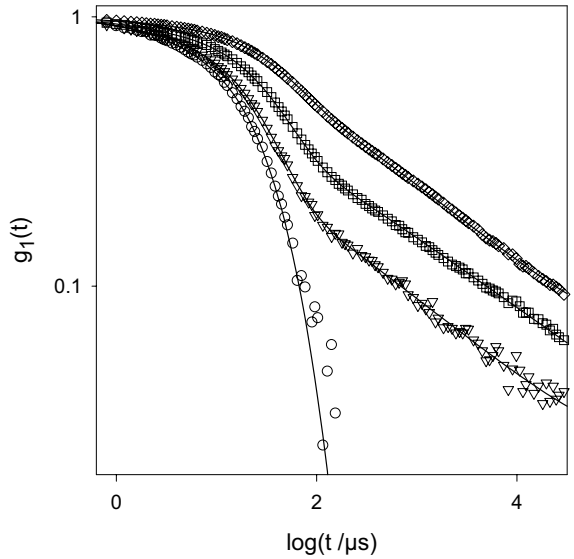

Fig. 8. Double logarithmic representation of the normalized electric field autocorrelation functions of solutions containing MMA and various amounts of cross linker EGDMA (R = [EGDMA]/[MMA]) close to the gel point. The data are obtained from measurements at $q = 1.5 \times 10^{-2}$ nm^{-1}. Symbols as in Figure 1. Solid lines are non-linear least squares fits to model b (see Appendix A).

2 which are q^2-dependent. The cooperative diffusion coefficient ($D_c = (q^2\tau)^{-1}$) of MMA is about 2×10^{-9} m^2/s and depends only weakly on the reaction time and R. The relaxation time of mode 2 which characterizes PMMA segment concentration fluctuations decreases with increasing reaction time, see Figure 6. τ_2 is independent of the cross-link ratio at least up to $R = 0.03$. For $R = 0.05$ mode 2 could not be measured accurately, because its relative amplitude was very small and I_r varied strongly over 10 min periods during the whole measurement (see Fig. 1). At very short reaction times mode 2 is due to self diffusion of not yet cross-linked PMMA chains. Therefore, the value of τ_2 at short reaction times can be used to calculate the hydrodynamic radius of uncross-linked chains [8]: $R_h = 6.5 \pm 0.5$ nm. This value is close to the value found for dilute solutions in THF of linear PMMA with the same M_w: $R_h = 6$ nm [7]. The corresponding value of R_g was reported to be 10 nm [7].

The average relaxation time of mode 3 (τ_3) is shown in Figure 7 as a function of t_r for different cross-link ratios. The values of τ_3 are uncertain because τ_3 is sensitive to the long time dependence of $g_1(t)$ where the noise level is important especially close to the gel point. In addition, close to the gel point the long time dependence of $g_1(t)$ evolves strongly during the 10 min measurements. Nevertheless, it is clear that τ_3 increases dramatically when the gel point is approached. For $R > 0.01$ very slow intensity fluctuations appear immediately after the gel point leading to a large base line on $g_2(t)$. For $R = 0.01$ and 0.005 these fluctuations are still very small just after the gel point. For these samples there is no doubt that τ_3 does not diverge at the gel point.

Figure 8 shows correlograms for systems close to the gel point at different values of R. It is clear that the relative amplitude of mode 3 (A_3) increases with increasing R. As explained in the Appendix A, A_3 cannot be determined unambiguously. It depends on the choice of the short time cut-off of the relaxation time distribution. With methods b and c this cut-off is forced at τ_2, while with method a the short time cut-off is situated at somewhat longer times. As a consequence methods b and c yield about the same values for A_3 while method a gives systematically smaller values. It turns out that I_e is the same as the fraction of I_r that relaxes slowly ($I_r A_3/(A_2 + A_3)$) if we use the amplitudes from methods a or b, see Figure 3.

To study the q-dependence of $g_1(t)$ we quenched the system close to the gel point by rapid cooling which practically stops the reaction. I_r decreases by about a factor of two when going from 68 °C to 20 °C. The decrease is independent of R which means that the temperature dependence of the contrast of PMMA and branching points is the same. We measured $g_1(t)$ at 20 °C as a function of q between 5×10^{-3} and 4×10^{-2} nm^{-1} ($16° \leq \theta \leq 150°$). Figure 9a shows the q-dependence of a system with $R = 0.01$. Figure 9b shows the same data as a function of $t \sin^2(\theta/2)$. In this representation diffusive modes decay at the same normalized time. This is the case for the first two modes but clearly not for the terminal relaxation time. Up to $q^{-1} \approx 100$ nm ($\theta = 30°$) the terminal relaxation time (and also τ_3) has a q^3-dependence, see inset in Figure 9b. At smaller q, *i.e.* when probing larger scale dynamics, we observe an increasingly sharp long time cut-off which appears to be q^2-dependent. We found a similar behaviour for the system with $R = 0.03$ close to the gel point.

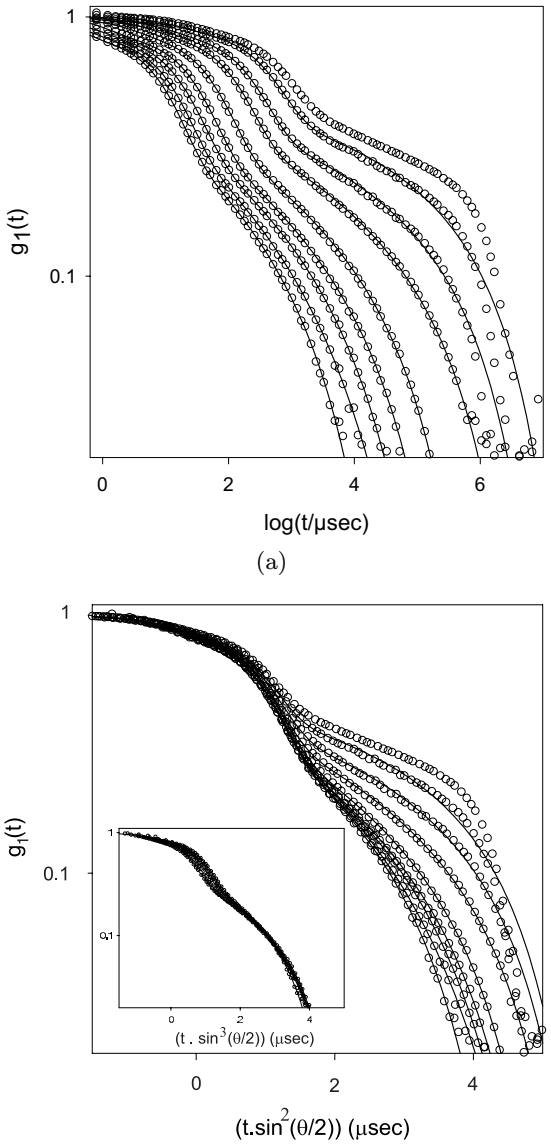

Fig. 9. (a) Double logarithmic representation of the q-dependence of the normalized electric field autocorrelation functions of a solution containing MMA and EGDMA with molar ratio $R = 0.01$ close to the gel point. The values of q vary between 5×10^{-3} and 4×10^{-2} nm^{-1} ($16° \leq \theta \leq 150°$). Solid lines are non-linear least squares fits to model b (see Appendix A). (b) Same data as in (a) as a function of $t \sin^2(\theta/2)$. In this representation q^2-dependent decays of $g_1(t)$ superimpose. The inset shows the data as a function of $t \sin^3(\theta/2)$ in the q-range 1×10^{-2} and 4×10^{-2} nm^{-1} ($30° \leq \theta \leq 150°$). Solid lines are non-linear least squares fits to model b (see Appendix A).

At earlier reaction times when τ_3 has not yet started to increase strongly τ_3 is q^2-dependent.

3.3 Effect of dilution

We investigated the effect of dilution for a sample with $R = 0.01$ very close to the gel-point. As the scattering contrast in toluene is small we did the dilution measurement for a sample prepared in THF and diluted with THF. The total scattering intensity increases strongly with increasing dilution. In addition, the intensity becomes increasingly q-dependent even in the range covered by light scattering. The q-dependence allowed us to extract an apparent radius of gyration ($R_{\rm ga}$) as a function of the concentration: $I_{\rm r} = I_{\rm r}(q \to 0)/[1 + (qR_{\rm gz})^2/3]$. These results have been reported earlier [9] and were found to be consistent with the scaling relation given in reference [10]. However, DLS measurements showed that the situation is more complicated. The undiluted sample in THF gave results which are similar to those obtained in toluene except that A_3 is about 0.35 instead of 0.5. Upon dilution A_3 increases while τ_3 decreases, see Figure 10. After dilution by more than a factor of three, modes 2 and 3 can no longer be clearly separated. As mentioned above A_2 and A_3 cannot be determined unambiguously. Using method b we obtained the values of A_3 shown in Figure 11. Method c gives the same results while method a gives systematically larger values. The uncertainty in the values becomes important if $A_2 < 0.3$ due to co-variation of fit parameters. Nevertheless, the strong increase of A_3 with dilution is obvious even from visual inspection of the data shown in Figure 10. Using DLS results we can identify the contribution of each mode to the total scattering: $I_2 = A_2 I_{\rm r}$ and $I_3 = A_3 I_{\rm r}$. The scattering from MMA concentration fluctuations is negligible in THF and $I_{\rm r} = I_2 + I_3$. The concentration dependence of $I_{\rm r}$, I_2 and I_3 extrapolated to $q = 0$ is shown in Figure 12. $I_2(q = 0)$ is only weakly concentration dependent and becomes negligible compared to I_3 after dilution by more than a factor of 10. Over the limited concentration range for which the analysis is accurate,

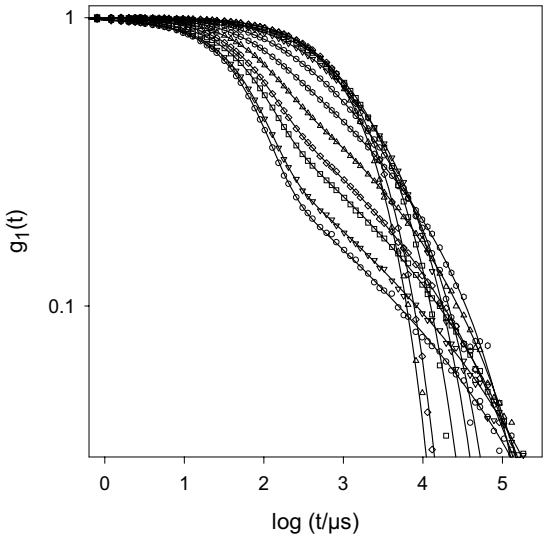

Fig. 10. Double logarithmic representation of the electric field autocorrelation functions of a solution containing MMA and EGDMA with molar ratio $R = 0.01$ close to the gel point at different polymer concentrations between 6.5×10^{-2} g/ml (undiluted) and 6.9×10^{-4} g/ml. For clarity only 1 in 3 data points is shown. Solid lines are non-linear least squares fits to model b (see Appendix A).

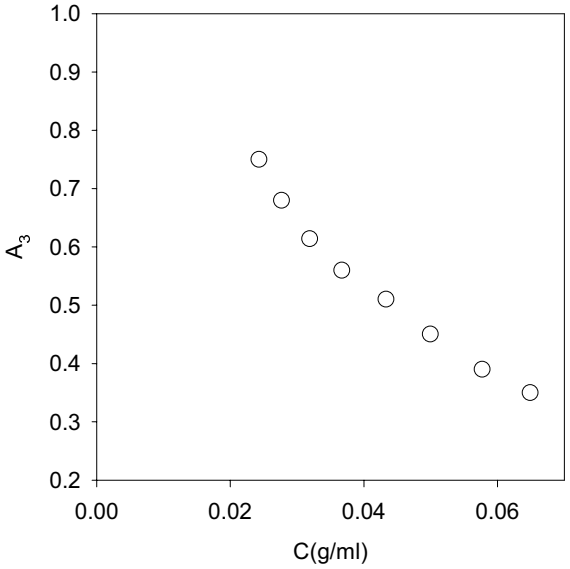

Fig. 11. Concentration dependence of the relative amplitude of scattering by branching points (mode 3).

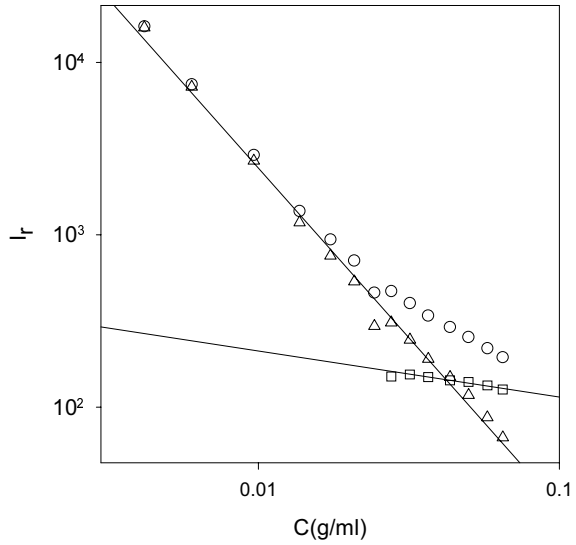

Fig. 12. Concentration dependence of the excess scattering intensity ($I_r = (I - I_{sol})/I_{tol}$) extrapolated to $q = 0$. Circles represent the total scattering, squares represent the contribution of mode 2 and triangles represent the contribution of mode 3. The solid lines represent linear least squares fits to the contributions of modes 2 and 3 and have slopes -0.26 and -2.00 respectively.

the concentration dependence of $I_2(q = 0)$ is close to that of semi-dilute solutions: $I \propto C^{-0.26}$. $I_3(q = 0)$ has a power law dependence on the concentration over the whole concentration range down to 4×10^{-3} g/ml: $I \propto C^{-2.0}$.

The q-dependence of I_2 is negligible while the q-dependence of I_3 increases with decreasing concentration. The q-dependence of I_3 at each dilution is close to that of I_r shown in reference [9], except at weak dilution when the contribution of I_2 cannot be neglected. After dilution by a factor of 1000 a power law behaviour is observed over

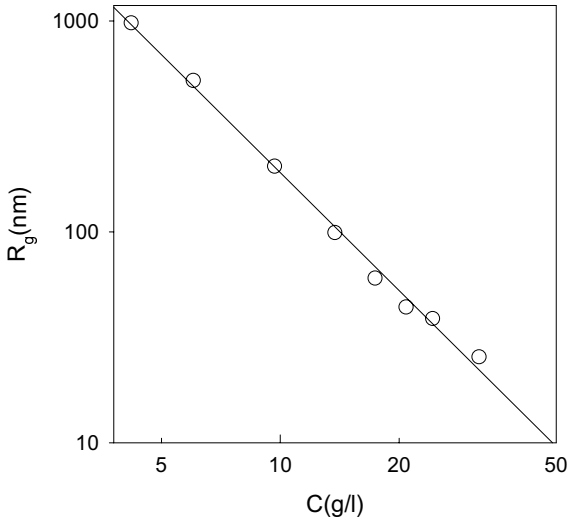

Fig. 13. Concentration dependence of the apparent radius of gyration. The solid line represents a linear least squares fit and has slope -1.86.

the whole accessible q-range: $I_r = I_3 \propto q^{-1.61}$. The data at each concentration were superimposed by normalizing q with R_{ga} and I_3 with $I_3(q = 0)$. In this way values for R_{ga} and $I_3(q = 0)$ can be obtained even if we cannot measure at low enough q for the Zimm approximation to be valid. We used the same procedure on highly diluted samples at different reaction times [3]. In the latter case R_{ga} is the z-average radius of gyration (R_{gz}) and $I_r(q = 0)$ is proportional to the weight average molar mass. The master curve obtained from the superposition represents the z-average structure factor of the system. We compare the structure factor of the semi-dilute system with that of the highly diluted system in reference [3]. The concentration dependence of R_{ga} is shown in Figure 13 and shows a power law dependence $R_{ga} \propto C^{-1.86}$ for $C < 0.03$ g/ml. At lower concentrations the concentration dependence of R_{ga} is weaker.

At all concentrations τ_2 is q^2-dependent and τ_3 is q^3-dependent. τ_2 increases weakly with decreasing concentration while τ_3 decreases initially, and then remains constant for $C < 7 \times 10^{-4}$ g/ml, *i.e.* dilution by more than a factor of 100.

4 Discussion

Two fundamentally different origins can be invoked for the excess scattering and the slow mode in cross-linked systems. On the one hand we can suppose that all the scattering is due to concentration fluctuations characterized by a single correlation length. In this case the excess scattering is due to a strong decrease of the osmotic modulus, *i.e.* the thermodynamic quality of the solvent. The relaxation process observed in DLS is then only determined by the relaxation of the longitudinal modulus $M(t)$ [2]. The longitudinal modulus is the sum of the osmotic and the elastic modulus which have different characteristic relaxation times. The relative amplitude of each mode

depends on the relative strength of the osmotic modulus compared to that of the elastic modulus [11]. This model has been used successfully to explain the molar mass and concentration dependence of the slow mode observed in semi-dilute linear polymer solutions close to theta conditions [12]. We believe, however, for reasons outlined below that the slow mode observed in cross-linked PMMA solutions is not due to visco-elastic relaxation of concentration fluctuations.

Firstly, visco-elastic relaxation is q-independent while we observe a strong q-dependence. Secondly, I_r increases strongly with increasing cross-link ratio while the cooperative diffusion coefficient ($D_\mathrm{c} = (q^2\tau_2)^{-1}$) is independent of R. This is incompatible with the model which predicts that $D_\mathrm{c} \propto M(t)$ and $I_\mathrm{r} \propto 1/M(t)$. Thirdly, τ_3 does not diverge at the gel point as predicted by the model. And finally, the strong increase of A_3 upon dilution in a good solvent is difficult to understand in terms of this model.

The second possibility, which we have already adopted in the results section, is that the excess scattering is due to the formation of branching points. The amount of excess scattering depends on the contrast of the branching points (K), the number of branching points (N_b), and the spatial distribution of the branching points. If we assume that the concentration fluctuations of PMMA segments and those of the branching points are not correlated then the total scattering is simply the sum of the two contributions. In general we can write the scattering intensity of the branching points as:

$$I_\mathrm{b} = KN_\mathrm{b}S_\mathrm{b}(q) \tag{2}$$

where $S_\mathrm{b}(q)$ is the structure factor which depends on the structure of the branching points and correlations between their center of mass positions. We have seen that in the q-range covered by light scattering the q-dependence is negligible so that $S_\mathrm{b}(q)$ is a constant. Neutron scattering measurements show that the correlation length of branching point concentration fluctuations (ξ_b) increases with increasing R [13]. However, ξ_b remains too small to give a noticeable q-dependence in the light scattering range at least up to $R = 0.03$. I_b can be identified with I_e and is shown as a function of t_r in Figure 3. At larger reaction times I_b remains approximately constant while N_b continues to increase. This implies that the increase of N_b is compensated by a decrease of K and/or S_b. The almost exponential increase of I_b with R is not simply due to an increase of N_b which is expected to be linear with R. The increase of I_b can only be explained by a strong increase of K and/or S_b with R. More measurements are needed to resolve these issues.

If we assume that the excess scattering is due to concentration fluctuations of branching points then mode 3 observed in DLS is due to the relative motion of branching points with respect to each other on the length scale of q^{-1}. Such a motion occurs either by self diffusion of the branched particles if $qR_\mathrm{g} < 1$ or by internal dynamics if the particles are flexible and $qR_\mathrm{g} > 1$. DLS measurements made on very dilute solutions show that the branched PMMA particles are completely flexible on the length scale probed by light scattering. The motion of branching points is, of course coupled to that of the branched particles. In order to quantify this motion we need to know the structure and size distribution of the particles formed during the gel formation.

Two theories have been proposed to describe the gel formation: mean field theory and percolation in three dimensions [14]. Mean field theory predicts that the density of branched particles increases with size. This is possible up to a certain extent if very large polymers are cross-linked, but becomes unphysical close to the gel point where the weight average particle size diverges. For many systems 3-d percolation is found to give a better description of the sol-gel transition. Both mean field theory and 3-d percolation predict a self similar structure and a power law molar mass distribution:

$$\begin{aligned} M &\propto R_\mathrm{g}^{d_\mathrm{f}} && M \gg M, \\ N(M) &\propto M^{-\tau} f(M/M^*) && M \gg M_0. \end{aligned} \tag{3}$$

Here d_f is the so-called fractal dimension, $f(M/M^*)$ is a cut-off function at a characteristic large molar mass M^*, M_0 is the molar mass of the elementary unit and τ is the polydispersity index not to be confused with the relaxation time. d_f can also be obtained from the particle structure factor at large qR_g. In practice, one measures the weight average molar mass, z-average radius of gyration and z-average structure factor in dilute solution. From these measurements one can determine an effective fractal dimension (d_f^*):

$$\begin{aligned} d_\mathrm{f}^* &= d_\mathrm{fs}(3-\tau) && \tau > 2 \\ d_\mathrm{f}^* &= d_\mathrm{fs} && \tau < 2 \end{aligned} \tag{4}$$

with d_fs the fractal dimension of the swollen particles after dilution. d_f has been related to d_fs using a mean field argument [15]. If one accepts this argument and knows τ independently, d_f can be calculated from d_f^*. We show in references [3,4] that the structure and size distribution of the PMMA aggregates is consistent with that of percolating clusters. The fractal dimension and the size distribution depend little on R in the range investigated.

To proceed further we need to assume that the number of branching points per particle is proportional to the molar mass of the latter ($N_\mathrm{b}(M) \propto M$) and that $S_\mathrm{b}(q)$ and K are independent of M. In this case the scattering amplitude due to branching points on particles with molar mass M is given by:

$$A(M) \propto MN(M) \propto M^{1-\tau} f(M/M^*) \quad M \gg M_0. \tag{5}$$

If $qR_\mathrm{g} < 1$ then the relaxation occurs through self diffusion of the particles and the relaxation time is given by: $\tau = (D_\mathrm{s}q^2)^{-1}$. The self diffusion coefficient (D_s) is inversely proportional to the friction coefficient which we assume to scale with R_g. It follows that:

$$\tau \propto q^{-2}R_\mathrm{g}^{\nu} \propto q^{-2}M^{\nu/d_\mathrm{f}} \qquad qR_\mathrm{g} < 1. \tag{6}$$

If $qR_\mathrm{g} > 1$ then the relaxation occurs through internal dynamics. The relaxation of internal dynamics is not a single

exponential, but the relaxation time distribution is relatively narrow and independent of M.

The distribution of relaxation times ($A(\log\tau)$) is obtained by changing variables: $M \rightarrow \log\tau$. We choose $\log\tau$ rather than τ as the variable because the measurements are done on a logarithmic time scale. If at a given value of q the characteristic radius of the largest particles (R_g^*) is less than q^{-1} then $A(\log\tau)$ becomes:

$$A(\log\tau)\mathrm{d}(\log\tau) \propto \tau^{d_f(2-\tau)/\nu} f(\tau/\tau^*)\mathrm{d}(\log\tau) \qquad \tau \gg \tau_0 \quad (7)$$

where $f(\tau/\tau^*)$ is the long time cut-off function at a characteristic slowest relaxation time

$$\tau^* \propto q^{-2}(R_g^*)^\nu \qquad qR_g^* < 1, \quad (8)$$

which decreases faster than any power law. τ_0 is the relaxation time of particles with molar mass M_0. If $R_g^* > q^{-1}$ we have to add the contribution of particles with $R_g > q^{-1}$, *i.e.* a relatively narrow relaxation time distribution. The ratio of the intensity scattered by branching points of all particles with $R_g > q^{-1}$ (I_l) to that of all particles with $R_g < q^{-1}$ (I_s) is given by:

$$\frac{I_l}{I_s} \propto \int_{M_1}^{M^*} M^{1-\tau}\mathrm{d}M \Big/ \int_{M_0}^{M_1} M^{1-\tau}\mathrm{d}M \quad (9)$$

where M_1 is the molar mass of the particles with size q^{-1}. If $\tau < 2$, I_l dominates, while if $\tau > 2$, I_s dominates provided $M_1 \gg M_0$. Regardless of the value of qR_g^*, $A(\log\tau)$ has a maximum close to τ^* if $\tau < 2$, and close to τ_0 if $\tau > 2$. In the case of cross-linked PMMA it is quite clear that the maximum of the slow relation time distribution is situated at short times implying $\tau > 2$ which is confirmed by SEC results on diluted samples [3,4]. The implication is that the only influence of particles larger than q^{-1} is on the cut-off function and that

$$\tau^* \propto q^{-3} \qquad qR_g^* > 1, \quad (10)$$

independent of R_g^*. Thus even in gels the terminal relaxation time remains finite. The reasoning given above was developed by Martin *et al.* [16] and was applied successfully to a number of systems [16,17]. The assumptions involved are reasonable for particles much larger than ξ_b. It is assumed that the branched particles although strongly overlapping are not entangled which is reasonable for percolating clusters [15].

To test the validity of the model for the present system we analyzed the data in terms of equation (7) using a stretched exponential cut-off function, *i.e.* equations (A.1, A.2) of the Appendix A (method *b*). It was shown in the Section 3 that the experimental data are well-described by this functional form except at very low scattering angles. In previous studies the contribution of the slow mode to $g_1(t)$ was fitted directly to the limiting behaviour of equation (7): $g_1(t) \propto kt^{-\alpha}$, which is valid for $t \ll \tau^*$ and again a stretched exponential cut-off (method *c*). The reason for using the limiting expression is that the fitting procedure is easier to implement and much faster. The difficulty for both methods is that the fit parameters are sensitive to the choice of the cut-off function. The model predicts correctly that the relative amplitude of mode 3 equals the excess intensity and that τ_3 has a q^3-dependence close to the gel point where $qR_g^* \gg 1$. However, the model does not explain the observations at very small scattering vectors.

As expected, values of τ^* obtained from the fits increase with increasing reaction time in the same way as τ_3. The values of the parameter p of equation (A.2) can only be obtained with some accuracy close to the gel point. We find $p = -0.15 \pm 0.1$ independent of R. The error bar is an estimation based on the results of different samples. There is no need to assume a dependence of p on the reaction time; a good fit is obtained if p is fixed at -0.15 in all cases. Comparison of equation (A.2) with equation (7) gives $p = d_f(2-\tau)/\nu$. Taking the values $d_f = 2.5$ and $\tau = 2.2$ from the percolation model we find $\nu = 3.3 \pm 1.5$. ν relates the self diffusion coefficient to the size: $D_s \propto R_g^{-\nu}$. Without hydrodynamic interactions (Rouse dynamics) ν equals d_f, *i.e.* $\nu = 2.5$, while in the case of non-draining (Zimm dynamics) $\nu = 1$.

Independent information on the dynamics can be obtained from viscosity measurements. If we assume that stress relaxation occurs through internal modes relaxation, the relaxation time of parts of size r and mass m is proportional to the time it takes to diffuse a distance r: $\tau \propto m^{(2+\nu)/d_f}$. Assuming power law polydispersity (Eq. (3)) it can be shown that the viscosity scales as: $\eta \propto M_w^\alpha$ with $\alpha = [d_f(1-\tau) + 2 + \nu]/d_f(3-\tau)$ [18], which simplifies to $\alpha = (1-\nu)/(3-2d_f)$ if we utilize the so-called hyper-scaling law $d_f(\tau - 1) = 3$. To obtain this result one has to assume again that the branched particles are not entangled. Figure 14 shows that the viscosity has indeed a power law dependence on the molar mass: $\eta = 0.10 M_w^{0.62\pm0.03}$ Pa s. Inserting values for d_f and τ from the percolation model we find $\nu = 2.2 \pm 0.1$. The results from rheology and DLS are within the experimental error consistent with each other and close to the value expected for *R*ouse dynamics.

It appears that the slow relaxation observed by DLS on systems close to the gel point can be consistently described in terms of self diffusion of branched particles which have a fractal structure and a power law size distribution. The terminal relaxation is determined by the diffusion of particles with size q^{-1}. Beyond the gel point an increasing fraction of the branching point density fluctuations cannot relax by this mechanism but relaxes much more slowly. Self diffusion over a length scale q^{-1} is to an increasing extent inhibited although not completely frozen. It is this increasingly slow relaxation that gives the slow variation of the scattering intensity after the gel point in Figure 1.

The results obtained on a progressively diluted sample show that the terminal relaxation time decreases with decreasing concentration. In addition, the data cannot be fitted correctly if we keep p fixed. We need to allow p to increase with decreasing concentration. Both observations imply that the self diffusion of the aggregates

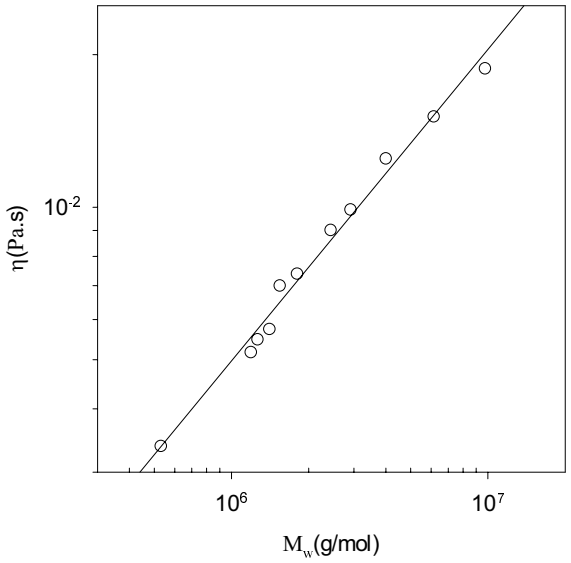

Fig. 14. Double logarithmic representation of the concentration dependence of the viscosity as a function of the weight average molar mass. The solid line represents a linear least squares fit and has slope 0.62.

becomes faster. Dilution decreases the degree of interpenetration of the branched particles and therefore the effect of hydrodynamic screening. Increasing hydrodynamic interactions leads to lower friction and therefore faster self diffusion. The decrease of the terminal relaxation time stabilizes when the particles are completely desinterpenetrated on the length scale q^{-1}.

Dilution leads to an increase of both $\xi_{\rm p}$ and $\xi_{\rm b}$. As long as $\xi_{\rm p}$ is smaller than the average distance between branching points ($l_{\rm b}$) the variation of $\xi_{\rm p}$ with concentration is similar to that of a semi-dilute solution of linear polymers. We should remember that at the gel point we still have a sizeable fraction of unbranched and weakly branched polymers. If $\xi_{\rm p}$ is much larger than $l_{\rm b}$ one expects that a single correlation length characterizes the system, *i.e.* $\xi_{\rm p} = \xi_{\rm b} = \xi$. In this case the pair correlation function of the scattering units which can be branching points or monomers is given by:

$$g(r) \propto r^{d_{\rm f}^*-3} f(r/\xi) \qquad \xi \gg l_{\rm b} \tag{11}$$

with $f(r/\xi)$ a cut-off function which decreases faster than any power law function. Equation (11) simply means that for distances smaller that ξ, the system has the same structure as a dilute solution. The experimentally observed parameter $R_{\rm ga}$ is proportional to ξ with a proportionality factor of order unity that depends on $d_{\rm f}^*$ and the form of $f(r/\xi)$.

To calculate the concentration dependence of $R_{\rm ga}$ we will follow the argument given by Daoud and Leibler [10]. They reasoned that $R_{\rm ga}$ is independent of $R_{\rm gz}$ as long as the concentration is larger than the overlap concentration (C^*). C^* is the concentration at which the volume occupied by the sum of all particles equals the total volume:

$$C^* \cong \frac{\int MN(M)\mathrm{d}M}{\int R_{\rm g}^3 N(M)\mathrm{d}M}\,. \tag{12}$$

Furthermore it is assumed that $R_{\rm ga}$ is proportional to $R_{\rm gz}$ if $C = C^*$ and that $R_{\rm ga}$ scales with C so that

$$\frac{R_{\rm ga}}{R_{\rm gz}} \propto \left(\frac{C}{C^*}\right)^{\alpha} \tag{13}$$

independent of $R_{\rm gz}$. Utilizing equation (3) in equation (12) we find

$$C^* \propto (R_{\rm gz})^{d_{\rm fs}(\tau-1)-3} \qquad \text{for} \quad 3/d_{\rm fs}+1 > \tau \tag{14}$$

so that $\alpha = 1/[d_{\rm fs}(\tau-1)-3]$. Of course, the argument leading to $R_{\rm gz} \propto C^{1/[d_{\rm fs}(\tau-1)-3]}$ is reasonable only if $R_{\rm gz} \gg l_{\rm b}$ and $C \gg C^*$.

Experimentally we find $\alpha = -1.86$ for $R_{\rm ga} > 20$ nm. This result together with the experimental value of $d_{\rm f}^* = 1.67$ gives us two independent relations containing τ and $d_{\rm fs}$ which can be solved to give: $\tau = 2.19$ and $d_{\rm fs} = 2.07$.

If we accept equation (11), the concentration dependence of $I_{\rm r}(q = 0)$ follows from that of $R_{\rm ga}$ as $I_{\rm r}(q = 0)/C \propto R_{\rm ga}^{d_{\rm f}^*}$. We discuss this point in detail in reference [3].

5 Conclusion

The scattering from a gelling system of MMA and EGDMA contains contributions from both PMMA segment concentration fluctuations and branching point concentration fluctuations. Consequently the system contains two length scales which characterize the correlation lengths of each concentration fluctuation. In undiluted samples both correlation lengths are too small to be accessible to light scattering. The scattering by the branching points increases initially with reaction time, but reaches a plateau at longer reaction time. The plateau value increases exponentially with the relative amount of cross linker in the range investigated.

Branching point concentration fluctuations relax due to self diffusion of the branched particles. The terminal relaxation time does not diverge at the gel point, but is q^3-dependent. Correlograms obtained from DLS measurements could be well-adjusted to a theoretical expression which assumes (a) a power law size distribution, (b) a fractal structure of the branched particles and (c) a friction coefficient that scales with the radius. The results are compatible with a structure and size distribution of percolating clusters and a friction coefficient proportional to the molar mass of the particles, *i.e. R*ouse dynamics.

The viscosity scales with the weight average molar mass and the exponent is close to the value expected for percolating clusters with Rouse dynamics.

Progressive dilution of a system quenched close to the gel point shows a strong increase of the scattering intensity

and the apparent radius of gyration. This increase is due to the disinterpenetration of the particles. The concentration dependence of the intensity and the apparent radius of gyration is in quantitative agreement with a model that assumes that the particle size distribution and structure is like that of percolating clusters. The model is valid only if $R_{\rm ga}$ is much larger than the distance between branching points and experimentally deviations from the predicted concentration dependence are observed for small $R_{\rm ga}$.

Appendix A: DLS data analysis

We used three methods to analyze the experimental correlograms.

(a) We took the inverse Laplace transform (ILT) of the correlation functions using the REPES routine [19] to obtain the corresponding relaxation time distributions ($A(\log\tau)$):

$$g_1(t) = \int A(\log\tau)\exp(-t/\tau)\mathrm{d}\log\tau. \qquad \text{(A.1)}$$

This method does not presuppose a particular form for $A(\log\tau)$, but has a tendency to present broad single peaked asymmetric distributions by several narrow peaks or by a too symmetric single peak depending on the amount of smoothing used.

(b) We fitted the correlation functions to a sum of three distributions: two log-normal distributions to describe the two fast diffusive modes and a so-called generalized exponential (GEX) distribution to describe the slow mode. The GEX distribution has the following form:

$$A(\log\tau) = k\tau^p \exp[-(\tau/\tau^*)^s], \qquad \text{(A.2)}$$

i.e. a power law dependence with a stretched exponential cut-off. k is a normalization constant and τ^* is the characteristic relaxation time of the long time cut-off. General properties of the GEX distribution and its application to DLS have been given in reference [20]. Experimentally, we find that we have to include a short time cut-off at the relaxation time of the cooperative PMMA diffusion. This is especially important if $p < 0$.

(c) We fitted $g_1(t)$ directly to the following function:

$$g_1(t) = A_1\exp(-\tau/\tau_1) + A_2\exp(-\tau/\tau_2) + A_3\begin{cases} 1 & t < \tau_2 \\ kt^{-\alpha}\exp[-(t/\tau^*)^\beta] & t > \tau_2 \end{cases} \qquad \text{(A.3)}$$

again k is a normalization constant which ensures that the third term has value A_3 at $t = \tau_2$. The GEX distribution with $p = -\alpha$ and $s = \beta/(1-\beta)$ is equivalent to the third term in equation (A.3) for either $\tau_2 \ll t \ll \tau^*$ or $t \gg \tau^*$. However, calculations show that these conditions are difficult to reach in practice if α is close to zero.

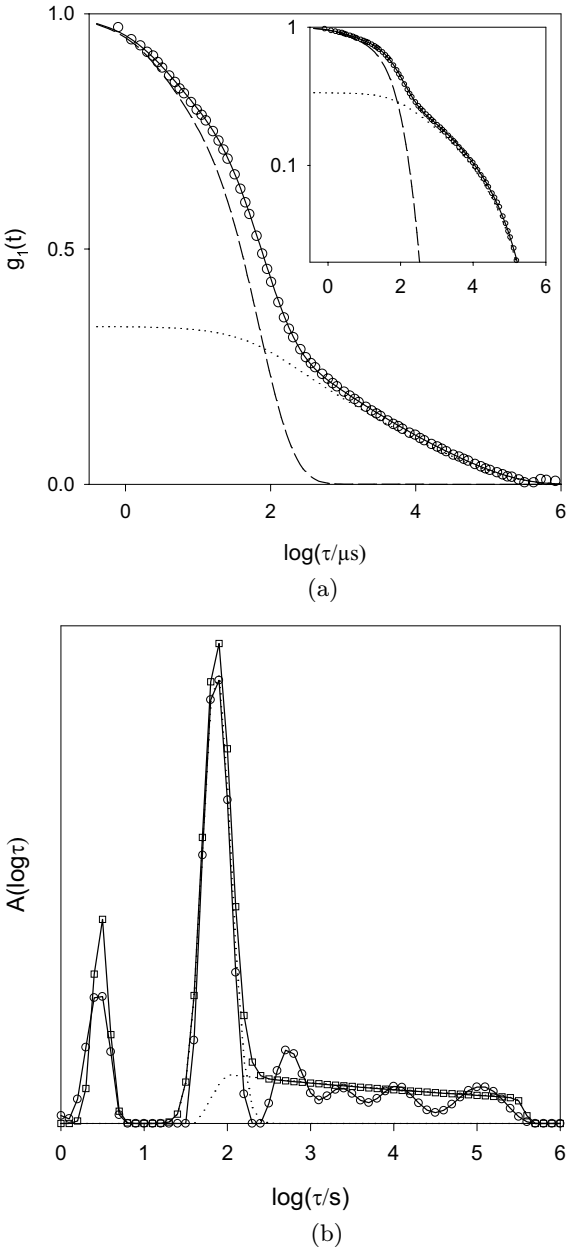

Fig. 15. (a) Example of a fit of the electric field autocorrelation function to method *b*. The dotted line represents the contributions of modes 1 and 2, while the dashed line represents the contribution of mode 3. (b) Comparison of relaxation time distributions corresponding to the correlation function shown in (a) obtained using methods *a* (circles) and *b* (squares). The dotted lines show the individual contributions of modes 2 and 3 in the analysis using method *b*.

The quality of the fits decreases when going from method *a* to *b* to *c*, but is still very good for method *c*. The analysis is illustrated in Figure 15a for a sample close to the gel point. The solid line shows the result from a fit using method *b*, but the result is indistinguishable from a fit using method *a* in this representation. The inset shows the same data in a double logarithmic representation. In this representation the slow mode is more clearly seen. That

is why in this paper correlograms are shown in this representation. Corresponding relaxation time distributions obtained from methods a and b are shown in Figure 15b. Both methods give a small peak at short times which corresponds to the relaxation of MMA concentration fluctuations and a large peak at longer times which corresponds to the relaxation of PMMA concentration fluctuations. Mode 3 is represented by a multiple peaked distribution using the REPES routine even with a probability to reject 0.5, while method b forces this distribution to be single peaked. The peak positions of the two diffusive modes (modes 1 and 2) are almost the same for the two methods. The mean relaxation time of mode 3 is the same within a factor 2 for the two methods, but is sensitive to experimental noise at large t and the presence of even a very small base line. We note that it is important to introduce the base line in $g_2(t)$ in the fit procedure. A slow drift in the intensity introduces a baseline in $g_2(t)$ and not in $g_1(t)$.

The main difference between the results from methods a and b are the relative amplitudes of modes 2 and 3. For the example shown in Figure 15 method a gives $A_2/(A_2 + A_3) = 0.23$ while method b gives 0.44. These values are not sensitive to the presence of a small base line. The difference is due to the fact that with method b the relaxation time distribution of the mode 3 starts at τ_2 and thus overlaps with the second peak of the REPES analysis, see Figure 15b. The main difficulty of the analysis is therefore the overlap of modes 2 and 3. This leads to considerable uncertainty in the relative amplitudes of these modes and some uncertainty in the relaxation time of the mode 3. Based on the experimental correlograms it is not possible to tell what is the short time cut-off of mode 3. Method c yields relaxation times and amplitudes very close to those obtained with method b.

References

1. J. Bastide, S.J. Candau, Structure of gels investigated by static scattering techniques, *Physical Properties of Polymer Gels*, edited by J.P. Cohen Addad (Wiley & Sons, Chicester, 1996).
2. A review is given in E. Geissler, Dynamic light scattering from gels, *Dynamic Light Scattering, the Method and some Applications*, edited by W. Brown (Clarendon Press, Oxford, 1993).
3. V. Lesturgeon, D. Durand, T. Nicolai, Eur. Phys. J. B **9**, 83 (1999).
4. C. Degoulet, T. Nicolai, J.P. Busnel, D. Durand, Macromolec. **28**, 6819 (1995).
5. S. Damoun, R. Papin, G. Ripault, M. Rousseau, J.C. Rabadeux, D. Durand, Raman Spectrosc. **23**, 385 (1992).
6. Y. Fujii, Y. Tamai, T. Konishi, H. Yamakawa, Macromolec. **24**, 1608 (1991).
7. P. Lang, W. Burchard, M.S. Wolfe, H.J. Spinelli, L. Page, Macromolec. **24**, 1306 (1991).
8. B. Berne, R. Pecora, *Dynamic light scattering* (Wiley, New York, 1976).
9. V. Lesturgeon, T. Nicolai, D. Durand, Europhys. Lett. **35** 573 (1996).
10. M. Daoud, L. Leibler, Macromolec. **21** 1497 (1988).
11. A.N. Semenov, Physica A **166**, 263 (1990); M. Doi, A. Onuki, J. Phys. II France **2**, 1631 (1992); U. Genz, Macromolec. **27**, 3501 (1994).
12. W. Brown, T. Nicolai, Dynamic properties of polymer solutions, *Dynamic Light Scattering, the Method and some Applications*, edited by W. Brown (Clarendon Press, Oxford, 1993).
13. J. Lal, J. Bastide, F. Boué, Macromolec. **26**, 6092 (993).
14. For a recent review see M. Adam, D. Lairez, Sol-gel transition, *Physical Properties of Polymer Gels*, edited by J.P. Cohen Addad (Wiley & Sons, Chicester, 1996).
15. M.E. Cates, J. Phys. Lett. France **46**, 757 (1985).
16. J.E. Martin, J.P. Wilcoxon, Phys. Rev. Lett. **61**, 373 (1988); J.E. Martin, J. Wilcoxon, J. Odinek, Phys. Rev. A **43**, 858 (1991).
17. P. Lang, W. Burchard, Macromolec. **24**, 814 (1991); L. Fang, W. Brown, C. Konak, Macromolec. **24**, 6819 (1991); J. Bauer, W. Burchard, J. Phys. II France **2**, 1053 (1992).
18. J.E. Martin, D. Adolf, J.P. Wilcoxon, Phys. Rev. Lett. **61**, 2620 (1988); M. Rubinstein, R.H. Colby, J.R. Gillmor, Dynamic scaling for Polymer gelation, *Space-Time Organization in Macromolecular Fluids*, edited by F. Tanaka, M. Doi, T. Ohta (Springer-Verlag, Berlin, 1989).
19. J. Jakes, J. Czech, J. Phys. B **38**, 1305 (1988).
20. T. Nicolai, J.C. Gimel, R. Johnsen, J. Phys. II France **6**, 697 (1996).